Recoil Polarization Measurements of the Proton Electromagnetic Form Factor Ratio to $Q^2 = 8.5\ \mathrm{GeV}^2$

A. J. R. Puckett,[1,*] E. J. Brash,[2,3] M. K. Jones,[3] W. Luo,[4] M. Meziane,[5] L. Pentchev,[5] C. F. Perdrisat,[5] V. Punjabi,[6] F. R. Wesselmann,[6] A. Ahmidouch,[7] I. Albayrak,[8] K. A. Aniol,[9] J. Arrington,[10] A. Asaturyan,[11] H. Baghdasaryan,[12] F. Benmokhtar,[13] W. Bertozzi,[1] L. Bimbot,[14] P. Bosted,[3] W. Boeglin,[15] C. Butuceanu,[16] P. Carter,[2] S. Chernenko,[17] E. Christy,[8] M. Commisso,[12] J. C. Cornejo,[9] S. Covrig,[3] S. Danagoulian,[7] A. Daniel,[18] A. Davidenko,[19] D. Day,[12] S. Dhamija,[15] D. Dutta,[20] R. Ent,[3] S. Frullani,[21] H. Fenker,[3] E. Frlez,[12] F. Garibaldi,[21] D. Gaskell,[3] S. Gilad,[1] R. Gilman,[3,22] Y. Goncharenko,[19] K. Hafidi,[10] D. Hamilton,[23] D. W. Higinbotham,[3] W. Hinton,[6] T. Horn,[3] B. Hu,[4] J. Huang,[1] G. M. Huber,[16] E. Jensen,[2] C. Keppel,[8] M. Khandaker,[6] P. King,[18] D. Kirillov,[17] M. Kohl,[8] V. Kravtsov,[19] G. Kumbartzki,[22] Y. Li,[8] V. Mamyan,[12] D. J. Margaziotis,[9] A. Marsh,[2] Y. Matulenko,[19] J. Maxwell,[12] G. Mbianda,[24] D. Meekins,[3] Y. Melnik,[19] J. Miller,[25] A. Mkrtchyan,[11] H. Mkrtchyan,[11] B. Moffit,[1] O. Moreno,[9] J. Mulholland,[12] A. Narayan,[20] S. Nedev,[26] Nuruzzaman,[20] E. Piasetzky,[27] W. Pierce,[2] N. M. Piskunov,[17] Y. Prok,[2] R. D. Ransome,[22] D. S. Razin,[17] P. Reimer,[10] J. Reinhold,[15] O. Rondon,[12] M. Shabestari,[12] A. Shahinyan,[11] K. Shestermanov,[19,†] S. Širca,[28] I. Sitnik,[17] L. Smykov,[17,†] G. Smith,[3] L. Solovyev,[19] P. Solvignon,[10] R. Subedi,[12] E. Tomasi-Gustafsson,[14,29] A. Vasiliev,[19] M. Veilleux,[2] B. B. Wojtsekhowski,[3] S. Wood,[3] Z. Ye,[8] Y. Zanevsky,[17] X. Zhang,[4] Y. Zhang,[4] X. Zheng,[12] and L. Zhu[1]

[1]*Massachusetts Institute of Technology, Cambridge, Massachusetts 02139, USA*
[2]*Christopher Newport University, Newport News, Virginia 23606, USA*
[3]*Thomas Jefferson National Accelerator Facility, Newport News, Virginia 23606, USA*
[4]*Lanzhou University, Lanzhou 730000, Gansu, People's Republic of China*
[5]*College of William and Mary, Williamsburg, Virginia 23187, USA*
[6]*Norfolk State University, Norfolk, Virginia 23504, USA*
[7]*North Carolina A&T State University, Greensboro, North Carolina 27411, USA*
[8]*Hampton University, Hampton, Virginia 23668, USA*
[9]*California State University Los Angeles, Los Angeles, California 90032, USA*
[10]*Argonne National Laboratory, Argonne, Illinois, 60439, USA*
[11]*Yerevan Physics Institute, Yerevan 375036, Armenia*
[12]*University of Virginia, Charlottesville, Virginia 22904, USA*
[13]*Carnegie Mellon University, Pittsburgh, Pennsylvania 15213, USA*
[14]*Institut de Physique Nucléaire, CNRS/IN2P3 and Université Paris-Sud, Orsay Cedex, France*
[15]*Florida International University, Miami, Florida 33199, USA*
[16]*University of Regina, Regina, Saskatchewan S4S OA2, Canada*
[17]*JINR-LHE, Dubna, Moscow Region, Russia 141980*
[18]*Ohio University, Athens, Ohio 45701*
[19]*IHEP, Protvino, Moscow Region, Russia 142284*
[20]*Mississippi State University, Starkville, Mississippi 39762, USA*
[21]*INFN, Sezione Sanità and Istituto Superiore di Sanità, 00161 Rome, Italy*
[22]*Rutgers, The State University of New Jersey, Piscataway, New Jersey 08855, USA*
[23]*University of Glasgow, Glasgow G12 8QQ, Scotland, United Kingdom*
[24]*University of Witwatersrand, Johannesburg, South Africa*
[25]*University of Maryland, College Park, Maryland 20742, USA*
[26]*University of Chemical Technology and Metallurgy, Sofia, Bulgaria*
[27]*University of Tel Aviv, Tel Aviv, Israel*
[28]*University of Ljubljana, SI-1000 Ljubljana, Slovenia*
[29]*DSM, IRFU, SPhN, Saclay, 91191 Gif-sur-Yvette, France*
(Received 20 April 2010; published 18 June 2010)

Among the most fundamental observables of nucleon structure, electromagnetic form factors are a crucial benchmark for modern calculations describing the strong interaction dynamics of the nucleon's quark constituents; indeed, recent proton data have attracted intense theoretical interest. In this Letter, we report new measurements of the proton electromagnetic form factor ratio using the recoil polarization method, at momentum transfers $Q^2 = 5.2$, 6.7, and 8.5 GeV^2. By extending the range of Q^2 for which G_E^p is accurately determined by more than 50%, these measurements will provide significant constraints on models of nucleon structure in the nonperturbative regime.

DOI: 10.1103/PhysRevLett.104.242301 PACS numbers: 25.30.Bf, 13.40.Gp, 24.85.+p

The measurement of nucleon electromagnetic form factors, pioneered at Stanford in the 1950s, has again become the subject of intense investigation. Precise recoil polarization experiments [1] established conclusively that the proton electric form factor G_E^p falls faster than the magnetic form factor G_M^p for momentum transfers $Q^2 \geq 1\ \mathrm{GeV}^2$, in disagreement with results obtained from cross section measurements [2–5]. Precise data to the highest possible Q^2 are needed, for example, to test the onset of validity of perturbative QCD (pQCD) predictions for asymptotic form factor behavior [6], to constrain generalized parton distributions (GPDs) [7], and to determine the nucleon's model-independent impact parameter-space charge and magnetization densities [8].

The effect of nucleon structure on elastic electron-nucleon scattering at a spacelike momentum transfer $q^2 = -Q^2 < 0$ is described in the one-photon-exchange approximation by the helicity-conserving and helicity-flip form factors $F_1(q^2)$ (Dirac) and $F_2(q^2)$ (Pauli), or alternatively the Sachs form factors, defined as the linear combinations $G_E = F_1 - \tau F_2$ (electric) and $G_M = F_1 + F_2$ (magnetic), where $\tau \equiv Q^2/4M^2$ and M is the nucleon mass. Polarization observables, such as the beam-target double-spin asymmetry [9] and polarization transfer [10,11] provide enhanced sensitivity to the electric form factor at large Q^2 compared to cross section measurements, for which G_M becomes the dominant contribution. The polarization of the recoil proton in the elastic scattering of longitudinally polarized electrons from unpolarized protons has longitudinal (P_l) and transverse (P_t) components with respect to the momentum transfer in the scattering plane [11]. The ratio P_t/P_l is proportional to G_E^p/G_M^p:

$$R \equiv \mu_p \frac{G_E^p}{G_M^p} = -\mu_p \frac{P_t}{P_l} \frac{E_e + E_e'}{2M_p} \tan\frac{\theta_e}{2}, \qquad (1)$$

where μ_p is the proton magnetic moment, E_e is the beam energy, E_e' is the scattered e^- energy, θ_e is the e^- scattering angle, and M_p is the proton mass. Because the extraction of G_E^p from the ratio (1) is much less sensitive than the Rosenbluth method [12] to higher-order corrections beyond the standard radiative corrections [13], it is generally believed that polarization measurements provide the correct determination of G_E^p in the Q^2 range where the two methods disagree. Previously neglected two-photon-exchange effects have been shown to partially resolve the discrepancy [14], and are a highly active area of theoretical and experimental investigation.

The new measurements of G_E^p/G_M^p were carried out in experimental Hall C at Jefferson Lab. A continuous polarized electron beam was scattered from a 20 cm liquid hydrogen target, and elastically scattered electrons and protons were detected in coincidence. Typical beam currents ranged from 60–100 μA. The beam helicity was reversed pseudorandomly at 30 Hz. The beam polarization of typically 80%–85% was monitored periodically using Möller polarimetry [15].

Scattered protons were detected in the Hall C High Momentum Spectrometer (HMS) [16], a superconducting magnetic spectrometer with three focusing quadrupole magnets followed by a 25° vertical bend dipole magnet, operated in a point-to-point tune. Charged particle trajectories at the focal plane were measured using drift chambers, and their momenta, scattering angles, and vertex coordinates were reconstructed using the transport matrix of the HMS. For this experiment, the HMS trigger was defined by a coincidence between the pair of scintillator planes just behind the drift chambers and an additional scintillator paddle placed at the exit of the dipole. The size of this new paddle matched the acceptance of elastically scattered protons.

To measure the polarization of scattered protons, a double focal plane polarimeter (FPP) was installed in the HMS detector hut, replacing the standard Čerenkov detector and rear scintillators. The FPP consists of two retractable 50 $\mathrm{g\,cm^{-2}}$ CH_2 analyzer doors, each followed by a pair of large-acceptance drift chambers with an active area $164 \times 132\ \mathrm{cm}^2$. The tracks of protons scattered in the analyzer material were reconstructed with an angular resolution of approximately 1 mrad.

Scattered electrons were detected in a large-acceptance electromagnetic calorimeter (BigCal) positioned for each Q^2 to cover a solid angle kinematically matched to the $\approx$7 msr proton acceptance of the HMS, up to 143 msr at $Q^2 = 8.5\ \mathrm{GeV}^2$. BigCal was assembled from 1744 lead-glass bars stacked in a rectangular array with a frontal area of $1.2 \times 2.2\ \mathrm{m}^2$ and a thickness of approximately 15 radiation lengths. The trigger for BigCal was formed from analog sums of up to 64 channels, grouped with overlap to maximize the efficiency for electrons at high thresholds of nearly half the elastic e^- energy, used to suppress charged pions and low-energy backgrounds. The overdetermined elastic ep kinematics allowed for continuous *in situ* calibration and gain matching. The primary trigger for the experiment was a time coincidence between BigCal and the HMS within a $\pm$50 ns window.

Elastic events were selected by applying cuts to enforce two-body reaction kinematics. The electron scattering angle θ_e was predicted from the proton momentum p_p and the beam energy, and the azimuthal angle ϕ_e was predicted from ϕ_p assuming coplanarity of the electron and the proton. The predicted electron trajectory was projected from the interaction vertex to the surface of BigCal and compared to the measured shower coordinates. The small area of each cell relative to the transverse shower size resulted in coordinate resolution of 5–10 mm, corresponding to an angular resolution of 1–3 mrad, which matched or exceeded the resolution of the predicted angles from elastic kinematics of the reconstructed proton.

An elliptical cut $(\Delta x/x_{max})^2 + (\Delta y/y_{max})^2 \leq 1$ was applied to the horizontal and vertical coordinate differences $(\Delta x, \Delta y)$, where (x_{max}, y_{max}) are the Q^2-dependent, 3σ cut widths used for the final analysis. An additional cut was applied to the proton angle-momentum correlation $p_p - p_p(\theta_p)$ which further suppressed the inelastic background. No cut was applied to the measured e^- energy, because the BigCal energy resolution was insufficient to provide additional separation between elastic and inelastic events. Figure 1 illustrates the separation of the elastic peak in the $p_p - p_p(\theta_p)$ spectrum using BigCal.

The dominant background was hard-bremsstrahlung-induced π^0 photoproduction, $\gamma + p \to \pi^0 + p$, in the 2.3% radiation length cryotarget, with the proton detected in the HMS and one or two π^0 decay photons detected in BigCal. The kinematics of this reaction overlap with elastic ep scattering within experimental resolution for near-end point photons. The contribution of quasielastic Al$(e, e'p)$ scattering from the cryocell windows was also measured and found to be negligible after cuts. The total background including inelastic reactions and random coincidences was estimated as a function of $p_p - p_p(\theta_p)$, as shown in Fig. 1, using a two-dimensional Gaussian extrapolation of the $(\Delta x, \Delta y)$ distribution of the background into the cut region under the elastic peak. A Monte Carlo simulation of elastic ep scattering and π^0 photoproduction was performed as a check on the background estimation procedure. The two methods agreed at the 10% (relative) level for wide variations of the cuts.

The angular distribution of protons scattered in the CH_2 analyzers measures the polarization components at the focal plane. The polar and azimuthal scattering angles (ϑ, φ) of tracks in the FPP drift chambers were calculated relative to the incident track defined by the focal plane drift chambers. The measured angular distribution can be expressed in the general form,

$$N^{\pm}(p, \vartheta, \varphi) = N_0^{\pm} \frac{\varepsilon(p, \vartheta)}{2\pi}[1 + (c_1 \pm A_y P_y^{FPP}) \cos\varphi + (s_1 \mp A_y P_x^{FPP}) \sin\varphi + c_2 \cos(2\varphi) + s_2 \sin(2\varphi) + \cdots], \quad (2)$$

where $N_0^{\pm}$ is the number of incident protons in the $\pm$ beam helicity state, $\varepsilon(p, \vartheta)$ is the fraction of protons of momentum p scattered by an angle ϑ, $A_y(p, \vartheta)$ is the analyzing power of the $\vec{p} + CH_2$ reaction, and P_x^{FPP} and P_y^{FPP} are the transverse components of the proton polarization at the focal plane. $c_1, s_1, c_2, s_2, \ldots$ are the Fourier coefficients of helicity-independent instrumental asymmetries, which are canceled to first order by the helicity reversal. Figure 2 shows the measured helicity-dependent azimuthal asymmetry $f_+ - f_- = \frac{2\pi}{\Delta\varphi}[\frac{N_+(\varphi)}{N_0^+} - \frac{N_-(\varphi)}{N_0^-}] \approx \bar{A}_y[P_y^{FPP}\cos\varphi - P_x^{FPP}\sin\varphi]$, where $\Delta\varphi$ is the bin width, summed over all p and the ϑ range $0.5° \leq \vartheta \leq 14°$ outside which $A_y \approx 0$.

The extraction of P_t, P_l, and P_t/P_l from the measured asymmetry at the focal plane involves the precession of the proton polarization in the HMS magnetic field, governed by the Thomas-BMT equation [17]. The rotation of longitudinal P_l into normal P_x^{FPP} allows the simultaneous measurement of P_t and P_l in the FPP, which is insensitive to longitudinal polarization. The unique spin transport matrix for each proton trajectory was calculated as a function of its angles, momentum, and vertex coordinates from a detailed model of the HMS using the differential-algebra based COSY software [18]. The polarization components at the target were then extracted by maximizing the likelihood function defined as

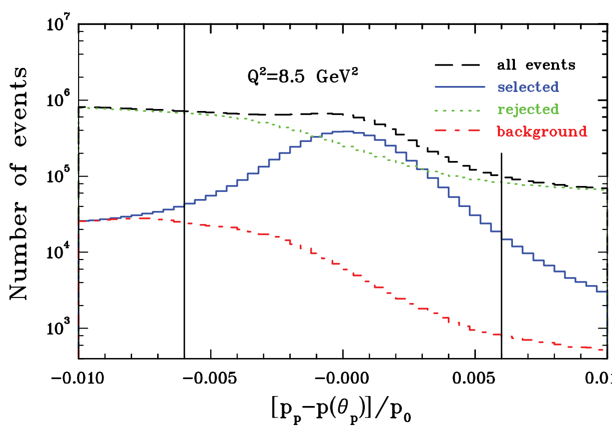

FIG. 1 (color). Elastic event selection for $Q^2 = 8.5$ GeV^2. The momentum difference $[p_p - p_p(\theta_p)]/p_0$, where p_0 is the HMS central momentum, plotted for all events (black dashed line), events passing the 3σ elliptical cut (blue solid line), and events failing the cut (green dotted line). The estimated background (red dot-dashed line) integrated over the final cut region (black vertical lines) is approximately 5.9%.

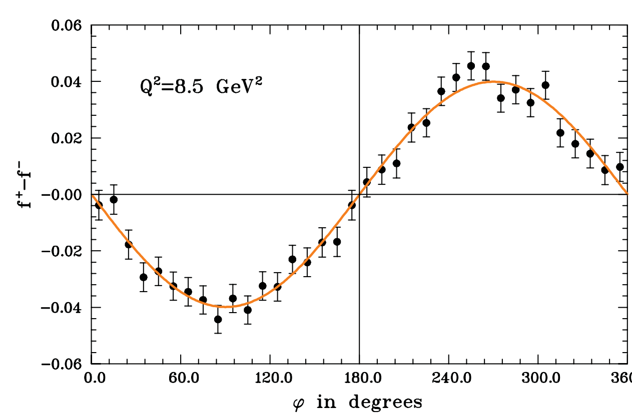

FIG. 2 (color). Helicity difference distribution $f_+ - f_-$ for $Q^2 = 8.5$ GeV^2, $0.5° \leq \vartheta \leq 14.0°$. The data are fitted with $f_+ - f_- = a\cos\varphi + b\sin\varphi$ (solid curve), resulting in $a = (0.16 \pm 1.19) \times 10^{-3}$ and $b = (-3.99 \pm 0.12) \times 10^{-2}$ $(\chi^2/\text{d.o.f.} = 0.67)$.

$$\mathcal{L}(P_t, P_l) = \prod_{i=1}^{N_{\text{event}}} [1 + h\epsilon_i A_y^{(i)} (S_{yt}^{(i)} P_t + S_{yl}^{(i)} P_l) \cos\varphi_i - h\epsilon_i A_y^{(i)} (S_{xt}^{(i)} P_t + S_{xl}^{(i)} P_l) \sin\varphi_i + \lambda_0^{(i)}], \quad (3)$$

where h is the beam polarization, $S_{jk}^{(i)}$ are the spin transport matrix elements, $\epsilon_i = \pm 1$ is the beam helicity, and λ_0 is the false asymmetry.

The polarization of the residual inelastic background passing "elasticity" cuts was obtained from the rejected events using the same procedure and used to correct the polarization of elastic events. The acceptance-averaged fractional inelastic backgrounds for $Q^2 = 5.2$, 6.7, and 8.5 GeV^2 were $N_{\text{inel}}/(N_{\text{inel}} + N_{\text{el}}) = (1.12 \pm 0.16)\%$, $(0.77 \pm 0.12)\%$, and $(5.9 \pm 0.9)\%$, respectively. The resulting absolute corrections to R were $\Delta R = (8.4 \pm 1.5) \times 10^{-3}$, $(7.5 \pm 1.3) \times 10^{-3}$, and $(6.0 \pm 1.3) \times 10^{-2}$.

Since the beam polarization and the $\vec{p} + CH_2$ analyzing power cancel in the ratio, there are few significant sources of systematic uncertainty in the results of this experiment. The most important contribution comes from the precession calculation. An excellent approximation to the full COSY calculation used for the final analysis is obtained from the product of simple rotations relative to the proton trajectory by angles χ_ϕ in the nondispersive plane and χ_θ in the dispersive plane. $\chi_\phi = \gamma\kappa_p\phi_{\text{bend}}$ and $\chi_\theta = \gamma\kappa_p\theta_{\text{bend}}$ are proportional to the trajectory bend angles ϕ_{bend} and θ_{bend} by a factor equal to the product of the proton's boost factor γ and anomalous magnetic moment κ_p. The relevant matrix elements in this approximation are $S_{yt} = \cos\chi_\phi$, $S_{yl} = \sin\chi_\phi$, $S_{xt} = \sin\chi_\phi \sin\chi_\theta$, and $S_{xl} = -\cos\chi_\phi \sin\chi_\theta$. These simple matrix elements were used to study the effects of systematic errors in the reconstructed kinematics.

The error $\Delta\phi_{\text{bend}}$ due to unknown misalignments of the quadrupoles relative to the HMS optical axis leads to an error $\gamma\kappa_p\Delta\phi_{\text{bend}}$ on P_t/P_l. This uncertainty was minimized through a dedicated study of the nondispersive optics of the HMS following the method of [19], setting a conservative upper limit of $|\Delta\phi| \leq 0.5$ mrad, which is the single largest contribution to the systematic uncertainty in R. The contribution of uncertainties in the absolute central momentum of the HMS and the dispersive bend angle θ_{bend} is small by comparison. The extracted form factor ratio showed no statistically significant dependence on any of the variables involved in the precession calculation, providing a strong test of its quality.

Uncertainties in E_e, E'_e, and θ_e make an even smaller contribution. Uncertainties in the scattering angles in the FPP were minimized by a software alignment procedure using "straight-through" data obtained with the CH_2 doors open. False asymmetry coefficients obtained from Fourier analysis of the helicity sum distribution $f_+ + f_-$ were used to correct the small, second-order contributions to the extracted polarization components. The resulting correction to R was small ($|\Delta R| \leq 0.007$) and negative for each Q^2. The correction procedure was verified using a Monte Carlo simulation.

The results of the experiment are presented in Table I. Standard radiative corrections to P_t/P_l were calculated using the code MASCARAD [13], found to be no greater than 0.13% (relative) for any of the three Q^2 values, and were not applied. Figure 3 presents the new results with recent Rosenbluth and polarization data and selected theoretical predictions.

Theoretical descriptions of nucleon form factors emphasize the importance of both baryon-meson and quark-gluon dynamics, with the former (latter) generally presumed to dominate in the low (high) energy limit. Recent vector meson dominance (VMD) model fits by Lomon [20] include $\rho'(1450)$ and $\omega'(1420)$ mesons in addition to the usual ρ, ω, and ϕ, and a "direct coupling" term enforcing pQCD-like behavior as $Q^2 \to \infty$. de Melo *et al.* [21] considered the nonvalence components of the nucleon state in a light-front framework, using *Ansätze* for the nucleon Bethe-Salpeter amplitude and a microscopic version of the VMD model. Gross and Agbakpe [22] modeled the nucleon as a bound state of three dressed valence constituent quarks in a covariant spectator theory. Cloët *et al.* [23] calculated a dressed-quark core contribution to the nucleon form factors in an approach based on Dyson-Schwinger equations in QCD. The disagreement between this calculation and the data at lower Q^2 is attributed to the omission of meson cloud effects.

The Dirac and Pauli form factors are related to the vector (H) and tensor (E) GPDs through sum rules [7]. Guidal *et al.* [24] fit a model of the valence quark GPDs based on Regge phenomenology to form factor data. In this model, the ratio F_2^p/F_1^p constrains the $x \to 1$ behavior of E, where x is the light-cone parton momentum fraction. When combined with the forward limit of H determined by parton

TABLE I. Results for $R = \mu_p G_E^p/G_M^p$, with statistical and systematic uncertainties. E_e is the beam energy, θ_e is the central electron scattering angle, $\langle Q^2 \rangle$ is the acceptance-averaged Q^2, and ΔQ^2 is the rms Q^2 acceptance.

E_e (GeV)	θ_e (°)	$\langle Q^2 \rangle \pm \Delta Q^2$ (GeV^2)	$R \pm \Delta R_{\text{stat}} \pm \Delta R_{\text{syst}}$
4.05	60.3	5.17 ± 0.123	$0.443 \pm 0.066 \pm 0.018$
5.71	44.2	6.70 ± 0.190	$0.327 \pm 0.105 \pm 0.022$
5.71	69.0	8.49 ± 0.167	$0.138 \pm 0.179 \pm 0.043$

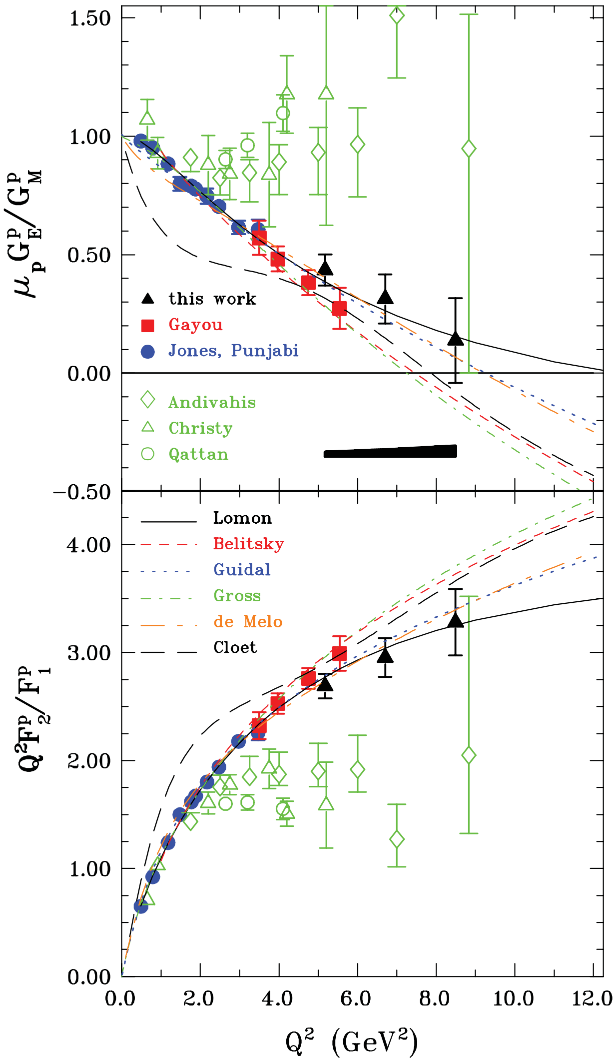

FIG. 3 (color). Upper panel: The proton form factor ratio $\mu_p G_E^p/G_M^p$ from this experiment (filled black triangles), with statistical error bars and systematic error band below the data. Previous experiments are [1] (Jones, Punjabi, Gayou), [3] (Andivahis), [4] (Christy), and [5] (Qattan). Theory curves are [20] (Lomon), [21] (de Melo), [22] (Gross), [23] (Cloët), [24] (Guidal), and [25] (Belitsky). Lower panel: The same data and theory curves as the upper panel, expressed as $Q^2F_2^p/F_1^p$.

distribution functions, the new information on E obtained from precise form factor data allowed an evaluation of Ji's sum rule [7] for the total angular momentum carried by quarks in the nucleon.

The data do not yet satisfy the leading-twist, leading order pQCD "dimensional scaling" relation $F_2^p \propto F_1^p/Q^2$ [6]. The modified scaling $Q^2F_2^p/F_1^p \propto \ln^2(Q^2/\Lambda^2)$ obtained by considering the subleading-twist components of the light-cone nucleon wave function [25], with $\Lambda = 300$ MeV as shown in Fig. 3, describes the polarization data rather well. This "precocious scaling" of F_2^p/F_1^p is a necessary, but not sufficient condition for the validity of a pQCD description of nucleon form factors. Despite progress in calculations based on light-cone QCD sum rules [26], pQCD form factor predictions have not yet reached the level of accuracy of phenomenological models such as [20–22,24] when applied to all four form factors ($F_{1,2}^{p,n}$), underscoring both the difficulty of predicting observables of hard exclusive reactions directly from QCD and the strong guidance to theory provided by high quality data such as the results reported in this Letter.

The collaboration thanks the Hall C technical staff and the Jefferson Lab Accelerator Division for their outstanding support during the experiment. This work was supported in part by the U.S. Department of Energy, the U.S. National Science Foundation, the Italian Institute for Nuclear Research, the French Commissariat à l'Energie Atomique and Centre National de la Recherche Scientifique (CNRS), and the Natural Sciences and Engineering Research Council of Canada. Authored by Jefferson Science Associates, LLC under U.S. DOE Contract No. DE-AC05-06OR23177.

*Corresponding author.
puckett@jlab.org
†Deceased.

[1] M. K. Jones *et al.*, Phys. Rev. Lett. **84**, 1398 (2000); V. Punjabi *et al.*, Phys. Rev. C **71**, 055202 (2005); O. Gayou *et al.*, Phys. Rev. Lett. **88**, 092301 (2002).
[2] C. Perdrisat, V. Punjabi, and M. Vanderhaeghen, Prog. Part. Nucl. Phys. **59**, 694 (2007).
[3] L. Andivahis *et al.*, Phys. Rev. D **50**, 5491 (1994).
[4] M. E. Christy *et al.*, Phys. Rev. C **70**, 015206 (2004).
[5] I. A. Qattan *et al.*, Phys. Rev. Lett. **94**, 142301 (2005).
[6] G. P. Lepage and S. J. Brodsky, Phys. Rev. Lett. **43**, 545 (1979).
[7] X. D. Ji, Phys. Rev. Lett. **78**, 610 (1997).
[8] G. A. Miller, Phys. Rev. Lett. **99**, 112001 (2007); G. A. Miller, E. Piasetzky, and G. Ron, *ibid.* **101**, 082002 (2008).
[9] N. Dombey, Rev. Mod. Phys. **41**, 236 (1969).
[10] A. I. Akhiezer and M. P. Rekalo, Sov. J. Part. Nucl. **3**, 277 (1974).
[11] R. G. Arnold, C. E. Carlson, and F. Gross, Phys. Rev. C **23**, 363 (1981).
[12] M. N. Rosenbluth, Phys. Rev. **79**, 615 (1950).
[13] A. Afanasev *et al.*, Phys. Rev. D **64**, 113009 (2001).
[14] C. E. Carlson and M. Vanderhaeghen, Annu. Rev. Nucl. Part. Sci. **57**, 171 (2007).
[15] M. Hauger *et al.*, Nucl. Instrum. Methods Phys. Res., Sect. A **462**, 382 (2001).
[16] H. P. Blok *et al.*, Phys. Rev. C **78**, 045202 (2008).
[17] V. Bargmann, L. Michel, and V. L. Telegdi, Phys. Rev. Lett. **2**, 435 (1959).
[18] K. Makino and M. Berz, Nucl. Instrum. Methods Phys. Res., Sect. A **427**, 338 (1999).
[19] L. Pentchev and J. LeRose, Report No. JLAB-TN-01-052, 2001.
[20] E. L. Lomon, Phys. Rev. C **66**, 045501 (2002); arXiv:nucl-th/0609020.

[21] J. P. B. C. de Melo, T. Frederico, E. Pace, S. Pisano, and G. Salmé, Phys. Lett. B **671**, 153 (2009).
[22] F. Gross and P. Agbakpe, Phys. Rev. C **73**, 015203 (2006); F. Gross, G. Ramalho, and M. T. Peña, *ibid.* **77**, 015202 (2008).
[23] I. C. Cloët, G. Eichmann, B. El-Bennich, T. Klähn, and C. D. Roberts, Few-Body Syst. **46**, 1 (2009).
[24] M. Guidal, M. V. Polyakov, A. V. Radyushkin, and M. Vanderhaeghen, Phys. Rev. D **72**, 054013 (2005).
[25] A. V. Belitsky, X. Ji, and F. Yuan, Phys. Rev. Lett. **91**, 092003 (2003).
[26] V. M. Braun, A. Lenz, and M. Wittmann, Phys. Rev. D **73**, 094019 (2006).